The Densities of Charged Particles in Very Dense Interstellar Clouds(Dissertation_全文)

AUTHOR(S):

Umebayashi, Toyoharu

学位申請論文

梅林豊治

論 文 内 容 の 要 旨

報告番号	甲第　　号	氏名	梅林豊治
論文調査担当者	主査　林　忠四郎 長谷川　博一　玉垣良三		

（論文題目）

The Densities of Charged Particles in Very Dense Interstellar Clouds.

（非常に密度の高い星間雲中での荷電粒子密度）

（論文内容の要旨）

星間雲から星が生まれるまでの重力収縮過程において，雲のもつ磁束がどのように漏出したかを明らかにすることは，星の形成，とくに主系列星のもつ磁場の起源の問題を解く上で極めて重要である。一般に，星間雲内の磁場はガスに凍結しており，この磁束を減少させる唯一の効果的な機構はプラズマ　ドリフトであると考えられている。すなわち，ガス雲の主成分である中性粒子は，自己重力のために，磁場が直接作用する荷電粒子の間をすり抜けて収縮しようとする。磁場の力は，荷電粒子との衝突を通して中性粒子にも働くが，この際に中性粒子のガスと荷電粒子のガスの間に速度差が生ずる。この速度差をもって雲の磁束が外部へ漏出して行く現象がプラズマ　ドリフトであって，その速度は星間雲中の荷電粒子の種類と存在量によって決定される。

主論文は，輻射を内部に閉じ込めうるような，非常に密度の高い星間雲

中の種々の荷電粒子の存在量を，雲が重力収縮の過程でたどる広範囲の密度　温度について，詳しく計算したものである。この荷電粒子の存在量は，低密度の星間雲の場合と同様に，宇宙線などによるガスの電離に始まるイオン　分子反応で決まる。申請者は，低密度の場合のイオン　分子反応系を，温度　密度の広い範囲で適用可能なものに拡張した。さらに，ガス中に含まれている固体微粒子の表面における，イオンと電子の再結合反応の重要性に着目して，この反応を上記の反応系に含めている。その結果，固体微粒子は，イオンと電子の再結合反応の場として重要であるだけでなく，荷電粒子の主要成分にもなっているという興味ある結論を得ている。

申請者はまず，微粒子表面で起こるイオンと電子の吸着と再結合の反応，さらに吸着粒子の脱着などの素過程を詳しく調べている。表面への吸着については，高温度になると，電子の吸着率は0.1以下に減少するが，イオンの吸着率はほぼ1のままであることを見出している。これは，電子は質量が小さいために，表面粒子との非弾性衝突によるエネルギー損失が起こりにくいためである。また，再結合反応については，気相中のイオンと電子が微粒子に衝突するときだけでなく，2個の微粒子が衝突する際に起こる吸着粒子の再結合も重要であることを指摘している。さらに，温度が数百度Kを超えると，微粒子表面に吸着されたイオンと電子が急速に蒸発しはじめることを見出している。

申請者は，上記の微粒子表面上の反応を含めたイオン　分子の反応系を構成し，その定常状態における荷電粒子密度を種々の温度　密度について計算した。その結果，脱着が重要でない低温の場合には，イオンと電子を各1個吸着した微粒子がほぼ同数存在し，これらが主要な荷電粒子になっていること，これに対応して，気相中のイオンと電子は小数成分となり，とくに電子の数密度はイオンの 1/200 に過ぎないことを見出している。このような荷電粒子の分布は，気相中のイオンと電子が主要成分である低

密度の場合とは全く異なっているが，申請はその理由を次のように説明している。すなわち，密度の増大に伴ってガスの電離度が低下して，電子とイオンの数密度が微粒子の数密度に近づいたために，気相中の電子の数が吸着によって大きい影響を受けるようになったことに起因している。さらに申請者は，温度上昇によって脱着が重要になると，帯電した微粒子の数は急送に減少して，気相中の電子とイオンが荷電粒子の主成分になることを見出している。

温度がさらに高い場合．ガスの電離は，宇宙線や放射線によるよりも熱電離による方がより重要になる。申請者は，荷電粒子密度に対する熱電離の影響を調べるために，熱電離によって決まるイオン密度を求め，これを上記の荷電粒子密度の計算結果と比較している。その結果，ガスの密度にはほとんど無関係に，温度がほぼ 1000K を超すと熱電離が最も重要になり，温度がさらに上昇すると，ガスの電離度が著しく増大することを推定している。

最後に，申請者は上記のイオン　分子反応系を原始星の収縮過程や原始太陽系星雲に適用し，これらの対象において，種々の荷電粒子の密度がどのような値をもつかを明らかにしている。

参考論文1は，主論文で取り扱った場合よりも低密度の星間雲について，微粒子の表面反応を含めてガスの電離度を調べたもので，主論文へと発展する前駆となったものである。参考論文2と3は，参考論文1で取り扱った低密度の星間雲中でのプラズマ　ドリフトを調べたものである。参考論文4は，主論文で取り扱った高密度の星間雲中での，宇宙線や放射性同位元素の放射線によるガスの電離過程を詳細に調べたものである。

主論文

The Densities of Charged Particles in Very Dense Interstellar Clouds

Toyoharu Umebayashi
Department of Physics, Kyoto University, Kyoto 606

Abstract

We examine the following processes on the grain surface: the adsorption of ions and electrons to the surface; the recombination of ions and electrons at grain-ion, grain-electron and grain-grain collisions; and the desorption of ions and electrons from the surface. As the temperature increases, the sticking probability of electrons to the surface is found to decrease to 0.1 or lower, while that of ions remains very close to unity. Above a certain critical temperature around several hundred kelvin, the desorption becomes abruptly efficient.

Solving the rate equations for chemical and grain-surface reactions, we investigate the abundances of various charged particles in very dense interstellar clouds (protostars). As long as the desorption is inefficient, grains with one excess ion and with one excess electron are the major constituents among charged particles

at densities higher than $10^{10}cm^{-3}$. Unlike the cases at lower densities, electrons and metal ions in the gas phase are only minor constituents, and it is found that the abundance of electrons is about 200 times smaller than that of metal ions. When the desorption becomes efficient, electrons and ions in the gas phase increase extensively as charged grains decrease. At the temperature above about 10^3K the thermal ionization dominates over the other processes of ionization, and the ionization degree increases extensively with the temperature.

§1. Introduction

The loss of magnetic flux from an interstellar cloud or from a part of a cloud is fundamental in the process of star formation. The only efficient process in reducing the magnetic flux of a cloud is the drift of plasma and magnetic field through the gas of neutral particles.[1] The time scale of magnetic flux loss due to this plasma drift is nearly proportional to the ion density for a cloud of relatively low density.[2] Because most grains are negatively charged in dense clouds shielded from the interstellar ultraviolet radiation, the friction between grains and neutrals also affects the plasma drift.[3] Recently Nakano[4] has investigated the quasistatic contraction of magnetic clouds including the effect of grain friction, and found that the density in the central part is about $10^9 cm^{-3}$ at the final stage of quasistatic contraction. In order to investigate the later stages of contraction we must obtain the densities of various kinds of charged particles at the densities above $10^9 cm^{-3}$.

The ionization degree at the density above $10^{11} cm^{-3}$ is also important in order to see the effects of magnetic fields on the primitive solar nebula.[5]

Many authors investigated the ionization degree in dense clouds using gas-phase reaction models with the recombination of ions and electrons on grains (Umebayashi and Nakano,[6] referred to as Paper I hereafter) and without one.[7] However, these works are restricted to the hydrogen densities $n_H \lesssim 10^9 cm^{-3}$.

Physical situations relevant to the ionization degree at $n_H \gtrsim 10^9 cm^{-3}$ are quite different from those at lower density in the following respects: (1) the ionization rate by cosmic ray begins to decrease exponentially as the column density of the cloud increases;[8] (2) because the number density of electrons, n_e, decreases to or below that of the negatively charged grains as the density increases, the charge neutrality requires that n_e becomes considerably less than the number density of ions, n_i, and then the charge state of grains changes; (3) since the clouds become opaque to the thermal radiation, the gas temperature increases with contraction.[9] We must take into account all the above effects on the ionization degree.

In this paper we shall investigate the densities of various charged particles in very dense interstellar clouds (protostars). In § 2 we examine the elementary processes for the charged particles and derive a simplified reaction scheme. Numerical results are presented in § 3. We investigate the effects of thermal ionization in § 4. In § 5 discussions are made on some related problems, and the reaction scheme is applied to the models of protostars and the primitive solar nebula.

§2. A model of the reaction system

As long as the gas temperature in a protostar is below about $10^3 K$, the gas is ionized mainly by cosmic rays and radioactive elements (see § 4). Then we can investigate the ionization degree

in the protostar, based on the ion-molecule reaction model in dense interstellar clouds. However, physical and chemical situations relevant to the ionization degree change extensively as the density and the temperature increase. Therefore, we survey the elementary reaction processes first, and construct a model for calculating the ionization degree in the protostars of relatively low temperature.

2.1 Adsorption of charged particles on grain surfaces

At the densities $n_H \gg 10^8 cm^{-3}$ the recombination of ions and electrons occurs mainly at the surface of grains. The sticking probability of various charged particles on grains is fundamental in this process. This process at low gas temperature ($T \lesssim 30$ K) was investigated in Paper I and the sticking probability was found to be close to unity. As the temperature rises, the sticking probability may decrease considerably, because the incident energies of charged particles on grains increase. Thus we estimate the change of the sticking probability with the temperature in the similar way as in Paper I.

When a charged particle of mass m approaches the surface of a grain with the initial incident energy E, it collides with a surface molecule and transfers some amount of energy to it (more exactly to lattice vibration). If such a collision can be regarded as the classical collision of the two free particles, the upper limit to the transferred energy is given by

$$\Delta E_s \simeq \frac{4m}{M_s}(E+D), \tag{1}$$

where M_s is the mass of the surface molecule, and D is the depth of the potential energy between the particle and the grain due to the electric polarization interaction and is a few eV. In the case when the incident particle is an electron, ΔE_s is much smaller than the energy quantum of the lattice vibration with the highest possible frequency. Thus the inelastic collision of an electron with a grain must be accompanied with the excitation of low-frequency phonons, which rarely occurs.

Using the phonon theory, we can obtain the probability of inelastic collision and the average energy transferred to the grain. Because the transferred energy in an inelastic collision is smaller than E (see Eq. (5) in Paper I), the electron usually hops translationally across the surface, making elastic and inelastic collisions before it finally escapes from the grain or becomes truely adsorbed. In this picture we easily obtain the adsorption probability of the electron (see Paper I for details)

$$P_e(E) \simeq \prod_{i=0}^{l-1} \frac{1}{1+\beta_i/\alpha}, \tag{2}$$

where α is the probability of inelastic collision, β_i is the probability with which the electron escapes from the surface in a hopping after the i-th inelastic collision, and l is the number of inelastic collisions needed in order that the electron is truely adsorbed.

The sticking probability $S_e(T)$ is the average of the adsorption probability $P_e(E)$ over the thermal energy distribution of the incident electrons,

$$S_e(T) = \int_0^\infty dE\, E\, exp(-\frac{E}{kT}) P_e(E) \Big/ \int_0^\infty dE\, E\, exp(-\frac{E}{kT}), \qquad (3)$$

where k is the Boltzmann constant. The sticking probability depends on the surface material of the grain through the mass of a surface molecule M_s [see Eq. (1)] and the Debye temperature (see Paper I). The results are shown in Figs. 1a and 1b for the grains whose surface is composed of graphite and ice, respectively. Since we do not know the exact value of D which depends on the physical and chemical conditions of the solid surface, we have calculated the cases of D = 1, 2, 3 and 4 eV. In all cases $S_e(T)$ is insensitive to the Debye temperature and the lattice size of the surface materials. At $T \lesssim 30$ K these results agree well with those in Paper I, where $P_e(\frac{3}{2}kT)$ is adopted as the sticking probability instead of taking the average over the energy distribution. Because the energy transfer in the inelastic collision is proportional to D (see Paper I), $S_e(T)$ decreases considerably as D decreases especially at high temperatures. Above a few hundred kelvin $S_e(T)$ becomes close to 0.1 or lower. Thus the incident electrons are scarcely adsorbed at such high temperatures.

Experiments on the sticking probability of electrons[10] have been done only at the electron energy $E \gtrsim 0.2$ eV, where the predominant interaction between electrons and solid surfaces is the

diffraction of electrons by ion cores rather than the energy transfer to phonons. These experiments also depend strongly on such surface conditions as the atom structure and contamination. Thus their results that the sticking probability is about 0.3 or higher do not contradict our results. If the collision of an incident electron with adsorbed particles on the surface sites is taken into account in our estimate, the sticking probability will become higher.

When an ion such as H^+, He^+, C^+, etc. collides with a grain, the energy transferred to the surface molecule ΔE_s is much larger than the energy quantum of the lattice vibration (see Eq. (1)). Then the inelastic collisions occur frequently, and the ion becomes bound to the surface after a few hoppings. Consequently the sticking probability of ions on grains is very close to unity, as long as the gas temperature is lower than several hundred kelvin.

Lastly, we briefly consider the effects of the excess charge of the grain on the sticking probabilities. Unless the number of the excess charges l in a unit of the electronic charge e is very large, or the radius of the grain, a, is very small ($a \lesssim 10^{-7}$cm), the average barrier of the electric potential at the surface is negligible compared with D (see Eq. (14) in Paper I). As will be seen below, l is not large and a is not so small. Therefore, when an electron collides with a negatively charged grain, and when an ion collides with a positively charged grain, the sticking probabilities differ little from those obtained above. On the other

hand, when an electron collides with a positively charged grain, or an ion collides with a negatively charged grain, the incident particle and one of the charged particles adsorbed on the grain approach to each other and finally recombine together. The resultant atom (or molecule) is likely to leave the surface (see Paper I and Watson and Salpeter[11]).

2.2 The charge-state distribution of grains

We consider next the charge-state distribution of grains in a protostar shielded from the ultraviolet radiation. From the discussion in § 2.1, we adopt the following model for surface reactions:

(1) The sticking probability of electrons on the neutral and negatively charged grains, S_e, varies from 1.0 to 0.1 or lower, as the temperature increases.

(2) The sticking probability of ions on the neutral and positively charged grains is unity at all the temperatures considered.

(3) When an ion hits a negatively charged grain, it recombines immediately with one of the adsorbed electrons, and the resultant atom or molecule leaves the surface.

(4) When an electron hits a positively charged grain, it recombines immediately with one of the adsorbed ions, and the resultant atom or molecule leaves the surface.

For simplicity, we regard both the shape of grains and the electric potential around charged grains as spherically symmetric.

As in the cases of lower densities, the metal ions such as Na^+, Mg^+, Ca^+ and Fe^+ are the overwhelming majority among the ions (see § 3). Therefore, we can neglect the contribution of the other ions.

Since most ions are singly charged in protostars, the transitions between the adjacent charge states of grains balance in the steady state. Introducing the relative number $N_l(a)$ of grains with radius a and charge le, the steady state is represented by

$$\langle \sigma v(a; l, l+1) \rangle_{M^+} n(M^+) N_l(a) = \mathcal{S}_e(l+1) \langle \sigma v(a; l+1, l) \rangle_e n(e) N_{l+1}(a), \tag{4}$$

where $n(M^+)$ and $n(e)$ are the number densities of metal ions M^+ and electrons, respectively, $\langle \sigma v(a; l, l') \rangle_X$ is the mean collision rate coefficient of a grain of radius a and charge le with the particle X, which is given by Eq. (15) or (16) in Paper I, and $\mathcal{S}_e(l)$ is the sticking probability of an electron hitting the grain of charge le. We take $\mathcal{S}_e(l) = 1.0$ for $l \geqq 1$, because the electron always recombines with one of the adsorbed ions.

This model for calculating the charge-state distribution of grains is essentially the same as that in Paper I. Consequently, as long as the number densities of ions and electrons are much higher than that of grains, the charge-state distribution is given by Fig. 1 of Paper I. At high densities, however, the densities of ions and electrons in the gas phase are affected extensively by their adsorption to grains. Thus we shall consider the other extreme case where the number density of charged grains is much higher than those of ions and electrons in the gas phase.

Because most of the charged grains have only one excess electron or metal ion, we have from charge neutrality $N_{-1}(a) \simeq N_1(a)$, as will be confirmed later. Then we can easily obtain from Eq. (4) the number ratio of electrons relative to metal ions in the gas phase

$$\frac{n(e)}{n(M^+)} = \left(\frac{1}{S_e}\frac{m_e}{m_M}\right)^{1/2}, \tag{5}$$

where m_e and m_M are the masses of the electron and the metal ion, respectively. Thus metal ions dominate over electrons in the gas phase.

Substituting Eq. (5) into Eq. (4), we obtain the ratio between the adjacent charge states

$$\frac{N_{l+1}(a)}{N_l(a)} = \frac{N_{-(l+1)}(a)}{N_{-l}(a)} = S_e^{1/2}\left[1+(l+1)\frac{e^2}{akT}\right]^{-1} exp\left(-\frac{le^2}{akT}\right), \tag{6}$$

where we assume $l \geqq 0$. Note that the ratio for positively charged grains has the same form as that for negatively charged grains. Both ratios depend on the temperature T and the grain radius a in the form of the product aT, which is similar to the cases in Paper I.

From Eq. (6) and the normalization condition ($\sum_{l=-\infty}^{\infty} N_l(a) = 1$) the charge-state distribution N_l is determined as a function of the product aT, and the results are shown in Fig. 2. Two cases $S_e = 1.0$ (Fig. 2a) and $S_e = 0.1$ (Fig. 2b) are shown in view of the change of

the sticking probability of electrons with the increase of the temperature. The charge-state distribution is found fairly sensitive to the sticking probability especially at $aT > 10^{-3}$cm K. Neutral grains are the most abundant even in the case $S_e = 1.0$. Most of the charged grains have one excess ion or electron. Grains with higher excess charges are only minor components in almost all the values of aT considered.

2.3 Grain-grain collisions

Since grains are in the thermal Brownian motion, they sometimes collide mutually. If the number densities of ions and electrons in the gas phase become extremely lower than that of grains, grain-grain collisions begin to occur more frequently than grain-ion and grain-electron collisions.

The time interval in which grains at the grain-grain collision make an interaction each other is approximately given by a/v_B, where v_B is the relative velocity of grains in the thermal Brownian motion. On the other hand, because grains rotate rapidly under random collisions with gas particles, the time required for the ions (or electrons) adsorbed on one grain to find out their companion for recombination on another grain is close to the rotation period of grain. The Coulomb force between the adsorbed ions and electrons will shorten this time scale. Since both time scales are essentially given by the same expression, we consider that the ions and electrons adsorbed on grains recombine each other during the grain-grain collision.

We can easily obtain the conditions that the time scale of the grain-grain collision becomes shorter than those of the grain-ion and grain-electron collision. The mean collision rate coefficient of a grain of radius a and charge le with another grain of raius a' and charge l'e is given by

$$\langle \sigma v \rangle_{gg} = \pi (a+a')^2 \left(\frac{8kT}{\pi\mu}\right)^{1/2} \left[1 - \frac{ll'e^2}{(a+a')kT}\right], \tag{7}$$

where μ is the reduced mass of the colliding grains, and we consider only the case $ll' \leqq 0$. Neglecting the effects of charges on grains, which are of minor importance, the above conditions for a = a' require

$$\frac{n(M^+)}{n_g} < 4 \left(\frac{2m_M}{m_g}\right)^{1/2}, \tag{8}$$

for the grain-ion collision, and

$$\frac{n(e)}{n_g} < 4 \left(\frac{2m_e}{m_g}\right)^{1/2}, \tag{9}$$

for the grain-electron collision, where n_g and m_g are, respectively, the number density and the mass of the grain. Because the densities of the electrons and ions in the gas phase satisfy Eq. (5), Eqs. (8) and (9) are substantially the same equation. As will be shown later, These conditions are satisfied at high densities. Therefore, we must take into account the recombination of adsorbed ions and electrons at grain-grain collisions.

For simplicity we adopt the following assumptions:

(1) We neglect the charge-transfer in collisions of grains

with the same sign of charges.

(2) In each collision, recombinations of all the adsorbed particles which can recombine at that collision occur.

(3) We neglect the coalescence of grains, although it might occur frequently.

2.4 Desorption of charged particles from grain surfaces

In a protostar with $n_H \gtrsim 10^{10}\text{cm}^{-3}$, the grain temperature is almost equal to the gas temperature.[12] Thus the desorption of particles bound to the grain surfaces becomes efficient with the increase of the temperature. For a neutral particle, the evaporation time is roughly given by

$$t_{ev} \simeq \nu_0^{-1} \exp(D/kT), \tag{10}$$

where ν_0 is the vibrational frequency of the adsorbed particle, and D is the adsorption binding energy (e.g., see Watson and Salpeter[11]). Although the situation for charged particles is different from that for neutral particles, we can estimate the evaporation time for a charged particle by using Eq. (10) with the appropriate values of ν_0 and D.

Table I shows the evaporation times t_{ev} for some values of D as a function of the temperature T. Here we simply adopt $\nu_0 = 10^{12}\text{s}^{-1}$, the characteristic lattice-vibration frequency of the solid. The evaporation time decreases extensively as T increases. At large D and low T the desorption is completely negligible. In

the region where the temperature in the protostar is above a few hundred kelvin, the number density of ions in the gas phase is about $10^{-5}cm^{-3}$ or higher, as will be confirmed in § 5.3. For the grain radius a = 10^{-5}cm, the time required for an ion to hit a grain is about 10^{10}s or shorter. Thus the desorption becomes abruptly efficient above a certain temperature, which strongly depends on D.

The actual values of the adsorption binding energy D and the vibrational frequency ν_0 for charged particles depend greatly on the chemical nature and surface condition of the grain, and on the kinds of adsorbed particles, particularly ions or electrons. Therefore, the desorption rate of each adsorbed particle varies extensively even at the same temperature. For simplicity, however, we include the desorption of charged particles in our reaction scheme, assuming that all the adsorbed particles have the same rate of desorption. The abundance of each charged particles is affected little by this assumption (see § 5.2).

2.5 A simplified reaction scheme

Now, let us construct a reaction model for calculating the densities of various kinds of charged particles in a protostar. The ion-molecule reaction scheme in dense interstellar clouds is the foundation of the reaction scheme in the protostar. As such a reaction scheme we adopt the simplified model of Paper I with some modifications about the treatment of the reactions concerned with grains.

The elements considered are H, He, C, O and metal M which is mainly composed of Na, Mg, Ca and Fe. The relative abundances of these elements adopted in this paper are the same as those in Table 3 of Paper I, which are essentially the solar abundances.[13] As in Paper I, two parameters are defined which represent the fractions of elements in the gas phase: δ_1 for C and O, and δ_2 for heavy metal atoms.

As for grains, we adopt the following model: (1) all grains have a radius a; (2) grains consist of such rocky and metallic materials as FeO, NiO, MgO and SiO_2.[14] Then we determine the number density of grains relative to hydrogen, n_g/n_H, assuming that the total missing amount of these elements (Mg, Si, Fe, Ni, etc.) in the gas phase relative to the solar abundance is all in the grains. Since most of these elements are depleted extremely even in the low density clouds,[15] we can regard that all of these elements are in the grains.

At low temperature grains also contain icy materials (H_2O, CH_4 and NH_3). Since the evaporation of these materials from grains become efficient above a certain temperature, the abundances of them in the gas phase increase and the grain radius decreases suddenly around such a temperature. The number density of grains may also change. In the following, however, we simply neglect these variations. We shall discuss their effects on the densities of charged particles in § 5.

As in dense interstellar clouds, we assume that all hydrogen is in the form of H_2. Almost all the carbon in the gas phase is in the form of CO or CH_4, and the oxygen in the gas phase other than the constituent of CO is in the form of O_2, H_2O, OH or O. The relative abundances of these molecules depend on the density and the temperature. Because the reaction rate coefficients of all these molecules with ions are of the same order, we neglect the change of these abundances, and the reactions of CO, O_2 and O are regarded as the representatives of their reactions. A parameter f_{O_2} which represents a fraction of oxygen in the form of O_2, H_2O and OH is taken as $f_{O_2} = 0.7$ in accordance with the molecule abundances calculated in dense clouds.[16] The change of the representatives and the value of f_{O_2} affect little the densities of charged particles.

In our simplified scheme the following species of charged particles are considered: electron e, H^+, He^+, C^+, H_3^+, molecular ions m^+ (except H_3^+) and metal ions M^+ in the gas phase, and grains of various kinds of charge states, G(l), where l is the charge of the grain in a unit of the electronic charge. As is seen from Fig. 1 in Paper I and Fig. 2, it is sufficient to include grains of charge states $|l| \leqq 3$. Because metal ions M^+ and molecular ions m^+ are the major constituents of ions (see § 3 and § 5.1), we assume that only these two kinds of ions are adsorbed on grain surfaces. Then we can easily include such reactions as grain-ion collisions, grain-electron collisions, grain-grain collisions and desorptions of ions and electrons from grain surfaces in our reaction scheme.

The main ion source is the ionization of H_2 and He by high-energy cosmic rays and radioactive elements. The products of the ionization of H_2 are H_2^+, which reacts immediately with H_2 to form H_3^+, and H^+ in the ratio of 97:3 (see Paper I). The ionization rate of He is given by 0.86ζ,[8] where ζ is the ionization rate of H_2.

The rate coefficients of ion-neutral reactions and ion-electron recombination reactions are shown in Tables 5 and 6 of Paper I. For some reactions we adopt the new data given by Prasad and Huntress.[17] Since the temperature considered is not much different from the room temperature, extrapolation or direct use of rate coefficients from laboratory measurements causes little difficulty. Three-body reactions, whose rate coefficients are of the order of $10^{-29}\mathrm{cm}^6\mathrm{s}^{-1}$,[18] are not included, because they are inefficient at densities $n_H \lesssim 10^{16}\mathrm{cm}^{-3}$ considered in this paper.

The rate equation for constituent X_i can be represented by

$$\frac{dn(X_i)}{dt} = \sum_j \gamma_{ij}\zeta n(X_j) + \sum_{j,k}\beta_{ijk}n(X_j)n(X_k) + \sum_j \eta_{ij}\kappa n(X_j), \quad (11)$$

where $n(X_i)$ is the number density of X_i, γ_{ij} is the constant factor for forming X_i by the ionization of X_j, β_{ijk} is the rate coefficient of the collisional reaction, κ is the desorption rate from grain surface, and η_{ij} is the constant factor for forming or extinguishing X_i by the desorption of X_j. In the steady state it follows from Eq. (11) that

$$\sum_j \gamma_{ij}\frac{\zeta}{n_H}x(X_j) + \sum_{j,k}\beta_{ijk}x(X_j)x(X_k) + \sum_j \eta_{ij}\frac{\kappa}{n_H}x(X_j) = 0, \quad (12)$$

where $x(X_j) \equiv n(X_j)/n_H$. From Eq. (12), the fractional abundance of any constituent, $x(X_j)$, depends only on ζ/n_H and $\mathcal{K}/n_H$.

§ 3. Numerical results

In numerical calculations we take the following values of the parameters. The depletion factors are taken as $\delta_1 = 0.2$ for C and O, and $\delta_2 = 0.02$ for heavy metal atoms. Taking the grain radius $a = 1\times10^{-5}$cm and the internal density within grain $\rho_s = 3$ g cm^{-3}, we find the relative number density of grains $n_g/n_H = 8\times10^{-13}$. As the column density of the cloud increases, the ionization rate of H_2, ζ, decreases from 1×10^{-17}s^{-1}, that by cosmic rays in interstellar clouds, to 7×10^{-23}s^{-1}, that by radioactive elements in the protostellar material.[8] Thus we calculate the abundances in the range of n_H/ζ between 10^{25} and 10^{40}cm^{-3}s. Another value $\mathcal{K}/n_H$ lies in the range between zero and 10^{-9}cm^{3}s^{-1}, since the desorption rate $\mathcal{K}$ is at most close to 1×10^{7}s^{-1} at high temperature (see Table I).

Figure 3 shows the relative abundances of various charged particles as a function of n_H/ζ for the cases without the desorption (i.e., $\mathcal{K} = 0$ s^{-1}). Here we have chosen the gas temperature T = 100 K and the sticking probability of electrons $S_e = 1.0$. For comparison the cases with and without grain-grain collisions are shown by the solid curves and the dashed curves, respectively. In both cases only the major constituents of ions and grains are shown for simplicity. Thus the abundances of positively charged grains are for grains which have adsorbed metal ions. The abundance of grains

with one excess molecular ion is, for instance, lower than that with one excess metal ion [the curve marked with G(+1)] by a factor of $x(M^+)/x(m^+)$. The abundances of ions in the gas phase $x(H^+)$, $x(C^+)$, etc. are also about 100 times lower than $x(m^+)$.

As long as $x(e) \simeq x(M^+) \gg n_g/n_H$, which is satisfied at $n_H/\zeta \lesssim 10^{27}\mathrm{cm}^{-3}\mathrm{s}$, both the ionization degree and the charge-state distribution of grains agree well with those in Paper I. At $n_H/\zeta \gtrsim 10^{27}\mathrm{cm}^{-3}\mathrm{s}$ $x(e)$ becomes lower than $x(M^+)$. The charge-state distribution of grains changes extensively up to $n_H/\zeta \simeq 10^{30}\mathrm{cm}^{-3}\mathrm{s}$. At $n_H/\zeta \gtrsim 10^{30}\mathrm{cm}^{-3}\mathrm{s}$ grains with one excess ion and with one excess electron become dominant among the charged particles, and the charge-state distribution of grains approaches that shown in Fig. 2a with $aT = 10^{-3}\mathrm{cm\ K}$. At $n_H/\zeta \gtrsim 10^{32}\mathrm{cm}^{-3}\mathrm{s}$, however, we have $x[G(+1)] \simeq x[G(-1)] \propto (n_H/\zeta)^{-1/2}$. This relation is derived by the following consideration. In such a region of n_H/ζ, where $x(M^+)$ and $x(e)$ fulfill Eqs. (8) and (9), respectively, the recombinations occur mostly at the grain-grain collisions. Therefore the balance of ionization and recombination is represented as

$$\frac{\zeta}{n_H} \simeq \langle \sigma v \rangle_{gg}\, x[G(+1)]\, x[G(-1)], \tag{13}$$

where $\langle \sigma v \rangle_{gg}$ is the rate coefficient of grain-grain collision given by Eq. (7). From Eq. (13) and the charge neutrality we have $x[G(+1)] \simeq x[G(-1)] \simeq (\zeta/n_H \langle \sigma v \rangle_{gg})^{1/2}$.

At $n_H/\zeta \gtrsim 10^{30}\mathrm{cm}^{-3}\mathrm{s}$ metal ion M^+ and electron e in the gas phase, whose abundances satisfy Eq. (5), are only the minor constituents

among the charged particles. In such a region of n_H/ζ the predominant reaction process of M^+ is the adsorption to neutral grains. Therefore, the rate equation for M^+ is approximately represented by

$$\frac{\zeta}{n_H} \simeq \langle \sigma v \rangle_{M^+} x(M^+) x[G(0)], \tag{14}$$

where $\langle \sigma v \rangle_{M^+}$ is the collision rate coefficient of a neutral grain with the metal ion M^+. Since $x[G(0)] \simeq n_g/n_H$, we have from Eq. (14) $x(M^+) \simeq \zeta/n_g \langle \sigma v \rangle_{M^+} \propto (n_H/\zeta)^{-1}$.

Now, let us consider the effects of the desorption on the relative abundances of charged particles. Figures 4 and 5 show the abundances with typical values of the desorption rate $\mathcal{K}/n_H$ as a function of n_H/ζ. We adopt $\mathcal{K}/n_H = 10^{-16}\mathrm{cm}^3\mathrm{s}^{-1}$ in Fig. 4 and $10^{-10}\mathrm{cm}^3\mathrm{s}^{-1}$ in Fig. 5. Other parameters are the same as in Fig. 3.

As is seen from Fig. 4, where the desorption is moderate, the ionization degree and the charge-state distribution of grains are affected little at $n_H/\zeta \lesssim 10^{27}\mathrm{cm}^{-3}\mathrm{s}$. At $n_H/\zeta \gtrsim 10^{30}\mathrm{cm}^{-3}\mathrm{s}$, however, the abundances of charged particles vary considerably. In such a region of n_H/ζ, where the abundances $x(e)$ and $x(M^+)$ are low, the desorption occurs more frequently than the grain-ion and grain-electron collisions. Thus the fractional abundances of charged grains are very small compared with those without the desorption. On the other hand, the abundances $x(e)$ and $x(M^+)$ become higher than those shown in Fig. 3.

Figure 5 shows the results with the very high desorption rate (see Table I). The case without grain-surface reactions (i.e., $\mathcal{K} = \infty\ s^{-1}$) is also shown for comparison by the dashed curves. In all region of n_H/ζ considered, the metal ion M^+ and electron e in the gas phase are the main constituents among charged particles. Although the fraction of negatively charged grains is extremely small, the recombination of ions and electrons occurs mostly at the grain surface.

In order to clarify further the effects of the desorption, we calculate the relative abundances as a function of $\mathcal{K}/n_H$, and the results are shown in Fig. 6. Here we choose $n_H/\zeta = 10^{35}cm^{-3}s$, and other parameters are the same as in Fig. 3. As long as $n_H/\zeta \gtrsim 10^{30}cm^{-3}s$ the results have similar shapes of the abundances.

At $\mathcal{K}/n_H \gtrsim 10^{-22}cm^3s^{-1}$, the desorption dominates over such reaction processes on grain surfaces as the recombination at the grain-ion, grain-electron and grain-grain collisions. Because the adsorption and desorption of ions at the grain surface balance in the steady state, we have

$$\langle\sigma v\rangle_{M^+} x[G(0)]x(M^+) \simeq \frac{\mathcal{K}}{n_H} x[G(+1)], \tag{15}$$

Using $x[G(0)] \simeq n_g/n_H$, we obtain the ratio $x[G(+1)]/x(M^+) \simeq \langle\sigma v\rangle_{M^+} n_g/\mathcal{K} \propto (\mathcal{K}/n_H)^{-1}$. Similarly we obtain the ratio $x[G(-1)]/x(e) \propto (\mathcal{K}/n_H)^{-1}$. In such a region of $\mathcal{K}/n_H$ the balance of ionization and recombination is described as

$$\frac{\zeta}{n_H} \simeq \langle\sigma v\rangle_e x[G(+1)]x(e), \tag{16}$$

where $\langle\sigma v\rangle_e$ is the collision rate coefficient of a positively charged grain with the electron. As long as $x[G(+1)] \simeq x[G(-1)] \gg x(M^+)$ which is satisfied at $\mathcal{K}/n_H \ll 10^{-17}cm^3s^{-1}$, we have from Eqs. (15) and (16) and the charge neutrality $x[G(+1)] \propto (n_H/\zeta)^{-1/2} x(\mathcal{K}/n_H)^{-1/2}$. At $\mathcal{K}/n_H \gg 10^{-15}cm^3s^{-1}$, where $x(e) \simeq x(M^+) \gg x[G(-1)]$, we have $x(e) \propto (n_H/\zeta)^{-1/2} (\mathcal{K}/n_H)^{1/2}$. At extremely high desorption rates $\mathcal{K}/n_H \gtrsim 10^{-8}cm^3s^{-1}$, the radiative recombination of metal ion becomes more efficient than the grain-surface recombination, and $x(e)$ and $x(M^+)$ approach a constant value given by the reaction model without grain-surface recombination.

Since the charge transfer reaction of m^+ with heavy metal atoms dominates over other reactions, $x(m^+)$ is constant in all region of $\mathcal{K}/n_H$.

§ 4. The effects of thermal ionization

As the gas temperature increases, the thermal ionization becomes efficient compared with the ionization by cosmic rays and radioactive elements. Thus at high temperature the thermal ionization affects extensively the densities of charged particles. In order to investigate this effect, we here take into account only the contributions of the thermal ionization, and calculate the abundances of ions in chemical equilibrium.

By considering the ionization potentials, the electron affinities and the abundances of various elements, we find it is sufficient to include only the elements Na, K and Cl in the gas phase,

and their ions Na^+, K^+ and Cl^- in the calculation. At the temperature $T \lesssim 10^3$K most of these elements are in condensates. Thus we must obtain the amount of them in the gas phase.

Assuming the complete chemical equilibrium between gases and condensates, Fegley and Lewis[19] have calculated the abundances of various gases and condensates of the elements Na, K, Cl, Br and P along the adiabat in their model of the primitive solar nebula. The abundances obtained by them are only functions of the thermodynamic state and are independent of the evolutionary path. Because their results are generally density-independent and their adiabat is close to the evolutionary path of protostars, we use their results so as to estimate the amount of Na, K and Cl in the gas phase.

Using these abundances, we can easily solve the ionization equilibrium of the elements mentioned above. In all the cases the reaction can be written as

$$A \rightleftharpoons B + e, \tag{17}$$

where A and B represent an atom and its ion. Then the equilibrium constant K can be defined by

$$K = P_A/P_B P_e, \tag{18}$$

where P_A, P_B and P_e are the partial pressures of species A, B and electron, respectively. Evaluating the equilibrium constant K from thermodynamic data and using the ideal gas law, we calculate the relative abundances of ions.

Figure 7 shows the abundance of ion K^+, $x(K^+) \equiv n(K^+)/n_H$, for the temperature between 600 K and 1400 K and the hydrogen density between $10^{10}cm^{-3}$ and $10^{16}cm^{-3}$. In most of the region considered, contours of the abundance of electron x(e) overlap with the contours of $x(K^+)$, and ions Na^+ and Cl^- are of minor importance.

Generally the results depend weakly on the density. As the temperature increases, the contribution of thermal ionization increases extensively, and at $T \gtrsim 10^3K$ the thermal ionization seems to be more efficient than the ionization by cosmic rays and radioactive elements (see § 5.3). Since the results in 3 depend strongly on n_H/ζ and $\mathcal{K}/n_H$, we cannot clarify the region where the thermal ionization becomes more efficient.

Above 10^3K most of the elements considered are in the gas phase. Thus the results at such temperatures are hardly affected by the abundances of elements in the gas phase. In all region shown in Fig. 7 each ion amounts to only a minor part of that element in the gas phase.

§ 5. Discussion and applications

5.1 Dependence on parameters

We first discuss the dependence of the results described in § 3 on the grain radius a, the temperature T and the sticking probability of electrons S_e. For this purpose we calculate the cases of $3\times10^{-6}cm \leq a \leq 3\times10^{-5}cm$, $10\ K \leq T \leq 10^3K$ and $0.01 \leq S_e \leq 1.0$, and find out that the change of these values affects little the basic

properties represented in Figs. 3 to 6. Quantitatively we obtain the following results:

(1) In case the desorption is negligible, the abundances x(e) and $x(M^+)$ change within a factor of 3, which can easily be estimated from Eqs. (14) and (5). As long as the grain-grain collision is inefficient, the charge-state distribution of grains approaches that given by Fig. 2 with appropriate values of aT and S_e. In the region of n_H/ζ where the grain-grain collision is the dominant process of recombinations, the abundances of the charged grains are obtained from Eq. (13).

(2) The desorption begins to dominate over other processes on grain surfaces at $\mathcal{K}/n_H$ between 10^{-23} and $10^{-20}cm^3s^{-1}$, which depends weakly on all of those parameters. Above such a value of $\mathcal{K}/n_H$ the abundances of major charged particles change within a factor of 3. These abundances are approximately derived by using Eqs. (15) and (16). The critical value of $\mathcal{K}/n_H$, above which the radiative recombination of metal ions becomes more efficient than the grain-surface recombination, varies between 10^{-9} and 10^{-6} cm^3s^{-1}.

At lower densities $n_H/\zeta \leq 10^{25}cm^{-3}s$ the ionization degree x(e) depends strongly on the depletion factor of metal δ_2 (see Fig. 2 in Paper I). At $n_H/\zeta \gtrsim 10^{27}cm^{-3}s$, however, the results for small desorption rates $\mathcal{K}/n_H \ll 10^{-13}cm^3s^{-1}$ shown in Figs. 3 and 4 change little even for the case $\delta_2 = 0$. The only change is that the ratio $x(m^+)/x(M^+)$ increases as δ_2 decreases. For $\delta_2 \ll 10^{-3}$ the molecular

ion m^+ becomes the main constituent among the ions in the gas phase, and most of the positively charged grains have molecular ions. On the other hand, for $\mathcal{K}/n_H \gg 10^{-13}\mathrm{cm}^3\mathrm{s}^{-1}$ the dissociative recombination of molecular ions becomes more efficient than the grain-surface recombination. Then similar to the cases of $n_H/\zeta \lesssim 10^{25}\mathrm{cm}^{-3}\mathrm{s}$, the ionization degree x(e) depends strongly on δ_2.

5.2 Reexamination of the assumptions about the grain-surface reactions

Since most of charged grains have only one excess ion or electron, the assumptions about the grain-grain collisions (see § 2.3) affect little the results shown in Fig. 3. The charge-transfer in collisions of grains with the same sign of charge may increase the abundances of grains with higher excess charge, but these grains are still the minor constituents among the charged grains. Since the rate coefficient for the charge-transfer reaction at grain-grain collision is much smaller than that for the recombination reaction, the abundances of grains with one excess ion and with one excess electron differ little from those given by Fig. 3.

The effects of the coalescence of grains can easily be estimated from the results for larger grain radius a (see § 5.1). In the region where the recombination at the grain-grain collisions is inefficient, the abundances of charged grains decrease as the grain radius a increases (i.e., the relative number of grains n_g/n_H decreases). However, when the grain-grain collisions become efficient,

these abundances are hardly affected. In all the region of n_H/ζ $x(e)$ and $x(M^+)$ are affected little by a and n_g/n_H. When the desorption is predominant, all the abundances depend weakly on a. Thus we can neglect the effects of the coalescence on the abundances obtained in § 3.

In § 2 and § 3 we have assumed that ions and electrons have the same desorption rate $\mathcal{K}$. In reality the precise values of $\mathcal{K}$ for ions and electrons are not known, and they may vary from grain to grain. Therefore, we have investigated the cases when the desorption rate of electrons $\mathcal{K}_e$ differs from that of ions $\mathcal{K}_i$ by many orders of magnitude. The results are summarized as follows: as long as both desorptions are efficient, the basic properties represented in Figs. 4 to 6 change little. The abundances of major constituents can be easily estimated from Eqs. (15) and (16) with appropriate values of $\mathcal{K}_e$ and $\mathcal{K}_i$. More important point about the desorption is when it becomes efficient (see § 5.3). Thus we can neglect the difference between $\mathcal{K}_i$ and $\mathcal{K}_e$ because of the uncertainties.

We have also neglected the evaporation of icy materials from grains. Such evaporation suddenly decreases a and n_g/n_H, and increases the fraction of elements C and O in the gas phase δ_1. From the discussion in § 5.1 (see also Fig. 9), the variation of a and n_g/n_H affects the abundances obtained in § 3 slightly. The increase of δ_1 merely affects the abundances of H^+, He^+, C^+ and H_3^+, which are the minor constituents of ions in the gas phase.

5.3 Applications

In the preceding sections, we have investigated the abundances of charged particles for arbitrary values of n_H/ζ and κ/n_H in very dense interstellar clouds. Now, we apply our reaction scheme to models of protostars and the primitive solar nebula. For this purpose we need the ionization rate of H_2, ζ, and the desorption rate κ as functions of the density n_H.

Using the column density x (in g cm^{-2}) traversed by cosmic rays to reach a place considered, the ionization rate is given by

$$\zeta(x) = \zeta_0 \exp(-x/\lambda) + \zeta_R, \tag{19}$$

where $\lambda \simeq 96$ g cm^{-2} is the attenuation length of the ionization rate, $\zeta_0 \simeq 1\times10^{-17}s^{-1}$ is the ionization rate by cosmic rays in the interstellar space and $\zeta_R \simeq 6.9\times10^{-23}s^{-1}$ is the ionization rate by radioactive elements.[8] As for the desorption rate we have from Eq. (10)

$$\kappa(T) \simeq 1/t_{ev} = \nu_0 \exp(-D/kT). \tag{20}$$

The sticking probability of electrons $S_e(T)$ is calculated by using Eq. (3). For simplicity we take the same value of the adsorption-potential depth D for $\kappa(T)$ and $S_e(T)$.

(i) Protostars

We take the following evolutionary paths of protostars: (1) paths given by Hattori et al.[9] in the transparent and early opaque stages; (2) paths of the cores obtained by Nakano et al.[20] in the

opaque stage where the contraction is nearly adiabatic. Since the above models of protostars are not extremely centrally condensed, we estimate the column density x at the center of protostars by assuming that protostars are spherically symmetric and their density distributions are uniform. Then the column density is given by

$$x = \left(\frac{3}{4\pi} M\right)^{1/3} \rho^{2/3} = 63 \left(\frac{M}{M_\odot}\right)^{1/3} \left(\frac{n_H}{10^{10} cm^{-3}}\right)^{2/3} g\ cm^{-2}, \tag{21}$$

where M and ρ are the mass and the density of the protostar, respectively.

For numerical computation we take the same values of the depletion factors and the same model of grains as in § 3. We choose the potential depth D = 2 eV for calculating $S_e(T)$ and $\mathcal{K}(T)$. The vibrational frequency of adsorbed particles $\nu_0 = 10^{12} s^{-1}$ is adopted.

The abundances of the major constituents for a protostar of mass $M = 1M_\odot$ are shown in Fig. 8 by solid curves together with the case without the desorption (dashed curves). The temperature T and the ionization rate $\zeta(x)$ are also shown in the upper side of the figure by dashed curves.

At $n_H \lesssim 10^{10} cm^{-3}$ electrons and metal ions in the gas phase are the most abundant and most grains have one excess electron. At $n_H \simeq 10^{10} cm^{-3}$, which corresponds to $n_H/\zeta \simeq 10^{27} cm^{-3} s$, x(e) approaches n_g/n_H and $\zeta(x)$ begins to decrease rapidly. Therefore, above $10^{10} cm^{-3}$, x(e) and $x(M^+)$ decrease extensively and grains with one excess electron and with one excess ion become dominant charged

particles. At $n_H \gg 10^{14} cm^{-3}$, where the temperature exceeds several hundred kelvin, the desorption becomes efficient (see Table I). Thus x(e) and $x(M^+)$ increase extensively with the decrease of the abundances of charged grains.

The results depend only weakly on the mass of protostar, because the effect of M is mainly through the ionization rate $\zeta(x)$. On the other hand, the critical temperature, where the desorption becomes efficient, depends strongly on D (see Table I). Thus the density at which x(e) and $x(M^+)$ begin to increase abruptly changes from $3 \times 10^{13} cm^{-3}$ for D = 1 eV to $1 \times 10^{15} cm^{-3}$ for D = 4 eV.

We can investigate the effects of thermal ionization by comparing the above results with those in Fig. 7. In Fig. 7 the evolutionary path of a protostar of $M = 1 M_\odot$ is also shown by a dashed curve. At $n_H \gtrsim 10^{15} cm^{-3}$, where T > 800K, the abundance of ions given by Fig. 7 is larger than that given by Fig. 8. Hence the thermal ionization becomes predominant above such temperatures, which are affected slightly by D. The ion density increases extensively with T after that.

At $n_H \gtrsim 10^{12} cm^{-3}$ the time required for the rate equations (11) to approach a steady state is very close to the free-fall time of protostars. Thus, it must be noted that Fig. 8 gives only an approximate account of the abundances of charged particles in protostars.

(ii) The primitive solar nebula

We investigate the densities of charged particles in the primitive solar nebula. We adopt the equilibrium model of the gaseous

nebula given by Hayashi.[5] In this model the gas surface density and the gas temperature are given, respectively, by

$$\rho_s(r) = 1.7 \times 10^3 \, r^{-3/2} \ \mathrm{g\ cm^{-2}}, \tag{22}$$

$$T(r) = 2.8 \times 10^2 \, r^{-1/2} \ \mathrm{K}, \tag{23}$$

where r is the distance from the sun (in astronomical unit). On the equatorial plane, where the ionization by the solar UV radiation is completely negligible, the density distribution of hydrogen is given by

$$n_H(r) = 6.4 \times 10^{14} \, r^{-11/4} \ \mathrm{cm^{-3}}. \tag{24}$$

We assume that grains have mantles of icy materials (H_2O, CH_4 and NH_3) at low temperature and their radius decreases as the temperature increases. This means that the grain radius is about two times larger than the core radius of grains in the outer region of the nebula, where the temperature is lower than the condensation temperature of icy materials. We consider the stages when the sedimentation of grains to the equatorial plane has not yet proceeded much.

The results are shown in Fig. 9. The value of the other parameters are the same as in Fig. 8. In most of the regions of the nebula charged grains are the major constituent among the charged particles, and electrons and ions in the gas phase are only the minor constituents. Because the radius of grains changes extensively in a narrow region around $r \simeq 3$ a.u., where the temperature

is about 160 K, $x(M^+)$ and $x(e)$ increase nearly discontinuously by a factor of 2. On the other hand, the abundances of charged grains are affected only slightly. In the region of terrestrial planets, where the ionization rate is very low by the attenuation of cosmic rays, the abundances of all charged particles, especially electrons and ions in the gas phase, decrease extensively. The abundance $x(M^+)$ generally agrees with the ionization degree estimated by Hayashi.[5]

Since the temperature is at most 500 K, the desorption is inefficient for $D \geqq 2$ eV throughout the nebula. If the potential depth D is as low as 1 eV, the desorption becomes a predominant process in the region inside Earth's orbit. In this case $x(e)$ and $x(M^+)$ in the regions of Mercury and Venus become much higher than those shown in Fig. 9.

Acknowledgements

The author wishes to thank Professor C. Hayashi for valuable discussions. He also thanks Professor T. Nakano for stimulating discussions, constructive suggestions and critical reading of the manuscript. He is indebted to the Japan Society for the Promotion of Science for financial aid. Numerical computations were performed at the Data Processing Center of Kyoto University. This work was supported partly by the Grant-in-Aid for Scientific Research of the Ministry of Education, Science and Culture (56540143).

References

1) L. Mestel and L. Spitzer, Jr., Month. Notices Roy. Astron. Soc. 116 (1956), 503.

2) See, for example, L. Spitzer, Jr., Physical Processes in the Interstellar Medium (John Wiley and Sons, 1978), p.293.

3) B.G. Elmegreen, Astrophys. J. 232 (1979), 729.
T. Nakano and T. Umebayashi, Publ. Astron. Soc. Japan 32 (1980), 613.

4) T. Nakano, Publ. Astron. Soc. Japan 34 (1982), 337; preprint KUNS 638 (1982), submitted to Publ. Astron. Soc. Japan.

5) C. Hayashi, Prog. Theor. Phys. Suppl. No.70 (1981), 35.

6) T. Umebayashi and T. Nakano, Publ. Astron. Soc. Japan 32 (1980), 405.

7) See, for example, M. Oppenheimer and A. Dalgarno, Astrophys. J. 192 (1974), 29.

8) T. Umebayashi and T. Nakano, Publ. Astron. Soc. Japan 33 (1981), 617.

9) T. Hattori, T. Nakano and C. Hayashi, Prog. Theor. Phys. 42 (1969), 781.

10) See, for example:
W.J. Fredericks and C.J. Cook, Phys. Rev. 121 (1961), 1693; J. Phys. Soc. Japan Suppl. II 18 (1963), 281.
J.J. Lander and J. Morrison, J. Appl. Phys. 35 (1964), 3593.

11) W.D. Watson and E.E. Salpeter, Astrophys. J. 174 (1972), 321.

12) C. Hayashi and T. Nakano, Prog. Theor. Phys. 34 (1965), 754.

13) A.G.W. Cameron, Space Sci. Rev. 15 (1973), 121.

14) M. Podolak and A.G.W. Cameron, Icarus 22 (1974), 123.

15) D.C. Morton, Astrophys. J. Letters 193 (1974), L35.

16) G.F. Mitchell, J.L. Ginsburg and P.J. Kuntz, Astrophys. J. Suppl. 38 (1978), 39.

17) S.S. Prasad and W.T. Huntress, Jr., Astrophys. J. Suppl. 43 (1980), 1.

18) L.A. Capone, R.C. Whitten, J. Dubach, S.S. Prasad and W.T. Huntress, Jr., Icarus 28 (1976), 367.

19) B. Fegley. Jr. and J.S. Lewis, Icarus 41 (1980), 439.

20) T. Nakano, N. Ohyama and C. Hayashi, Prog. Theor. Phys. 39 (1968), 1448.

Table I. The evaporation time of particles which are bound to the surface with the adsorption binding energy D and oscillate with the frequency $\nu_0 = 10^{12} s^{-1}$ as a function of the temperature T.

D (eV)	T (K)		
	200	500	800
1	1.5×10^{13}s	1.2×10^{-2}s	2.0×10^{-6}s
2	2.4×10^{38}	1.4×10^{8}	3.9
3	3.7×10^{63}	1.7×10^{18}	7.8×10^{6}
4	5.7×10^{88}	2.0×10^{28}	1.5×10^{13}

Figure Captions

Fig. 1. The sticking probabilities of electrons hitting the solid surface as functions of the temperature T. The properties of surface materials adopted are graphite (Fig. 1a) and ice (Fig. 1b). The value of the potential depth D is attached to each line.

Fig. 2. The charge-state distribution of grains. The relative number of grains N_1 with the charge le among the grains of the radius a is shown as a function of aT, the product of the radius a (in cm) and the gas temperature T (in kelvin), for the case when the number density of grains is much higher than that of ions and electrons in the gas phase. The sticking probability of electrons on neutral and negatively charged grains S_e is taken as 1.0 in Fig. 2a and 0.1 in Fig. 2b. All lines for negatively charged grains overlap with the lines for positively charged grains. The absolute value of the grain charge 1 is attached to each line.

Fig. 3. Relative abundances of various charged particles, $x(X) \equiv n(X)/n_H$, as a function of n_H/ζ, the total hydrogen density n_H (in cm^{-3}) divided by the ionization rate of a hydrogen molecule by cosmic rays and radioactive elements, ζ (in s^{-1}), for the following case: the solar abundance of the elements is adopted; fractions $\delta_1 = 0.2$ of C and O and $\delta_2 = 0.02$ of heavy metal atoms are in the gas phase; the radius of grains $a = 10^{-5}$cm; the gas temperature T = 100 K; the sticking probability

of electrons $S_e = 1.0$; the desorption of charged particles from grains is neglected. The abundances with and without the grain-grain collisions are shown, respectively, by the solid curves and the dashed curves.

Fig. 4. Relative abundances of various charged particles with the desorption of charged particles from grains. The desorption rate $\mathcal{K}$(in s^{-1}) divided by n_H, $\mathcal{K}/n_H = 10^{-16} cm^3 s^{-1}$ is adopted. Other parameters are the same as in Fig. 3.

Fig. 5. Relative abundances of various charged particles for the desorption rate $\mathcal{K}/n_H = 10^{-10}$ $cm^3 s^{-1}$. Other parameters are the same as in Fig. 3. The dashed curves represent relative abundances without the grain-surface reactions (i.e., $\mathcal{K} = \infty$ s^{-1}).

Fig. 6. Relative abundances of various charged particles for $n_H/\zeta = 10^{35} cm^{-3} s$ as a function of the desorption rate $\mathcal{K}/n_H$. Other parameters are the same as in Fig. 3.

Fig. 7. Contours of the relative abundance of the ion K^+ in the gas phase, $x(K^+) \equiv n(K^+)/n_H$, in the n_H-T diagram. Only the contribution of the thermal ionization is included. Contours are labeled with the values of log $x(K^+)$. The evolutionary path of a protostar of $1M_\odot$ (for details see § 5.3) is shown by the dashed curve.

Fig. 8. Relative abundances of the major kinds of charged particles along the evolutionary path of a protostar of $1M_\odot$ (for details see text). Parameters adopted are the same as in

Fig. 3 with the following exceptions: the sticking probability of electrons $S_e(T)$ is evaluated from Eq. (3); the desorption rate of charged particles $K(T)$ is calculated, using Eq. (20) with the vibrational frequency $\nu_0 = 10^{12} s^{-1}$; the well depth of adsorption potential D = 2 eV is adopted for calculating $S_e(T)$ and $K(T)$. The case without the desorption is shown for comparison by the dashed curves. The gas temperature T and the ionization rate $\zeta(x)$ evaluated from Eqs. (19) and (21) along the evolutionary path are also plotted by the dashed curves.

Fig. 9. Relative abundances of major charged particles on the equatorial plane of the primitive solar nebula[5] as a function of the distance from the sun r (in astronomical unit). Parameters adopted are the same as in Fig. 8. In the outer parts of the nebula where the gas temperature is lower than the condensation temperature of ice, grains are assumed to have ice mantles. The ionization rate $\zeta(x)$ evaluated from Eqs. (19) and (22) is shown by the dashed curve.

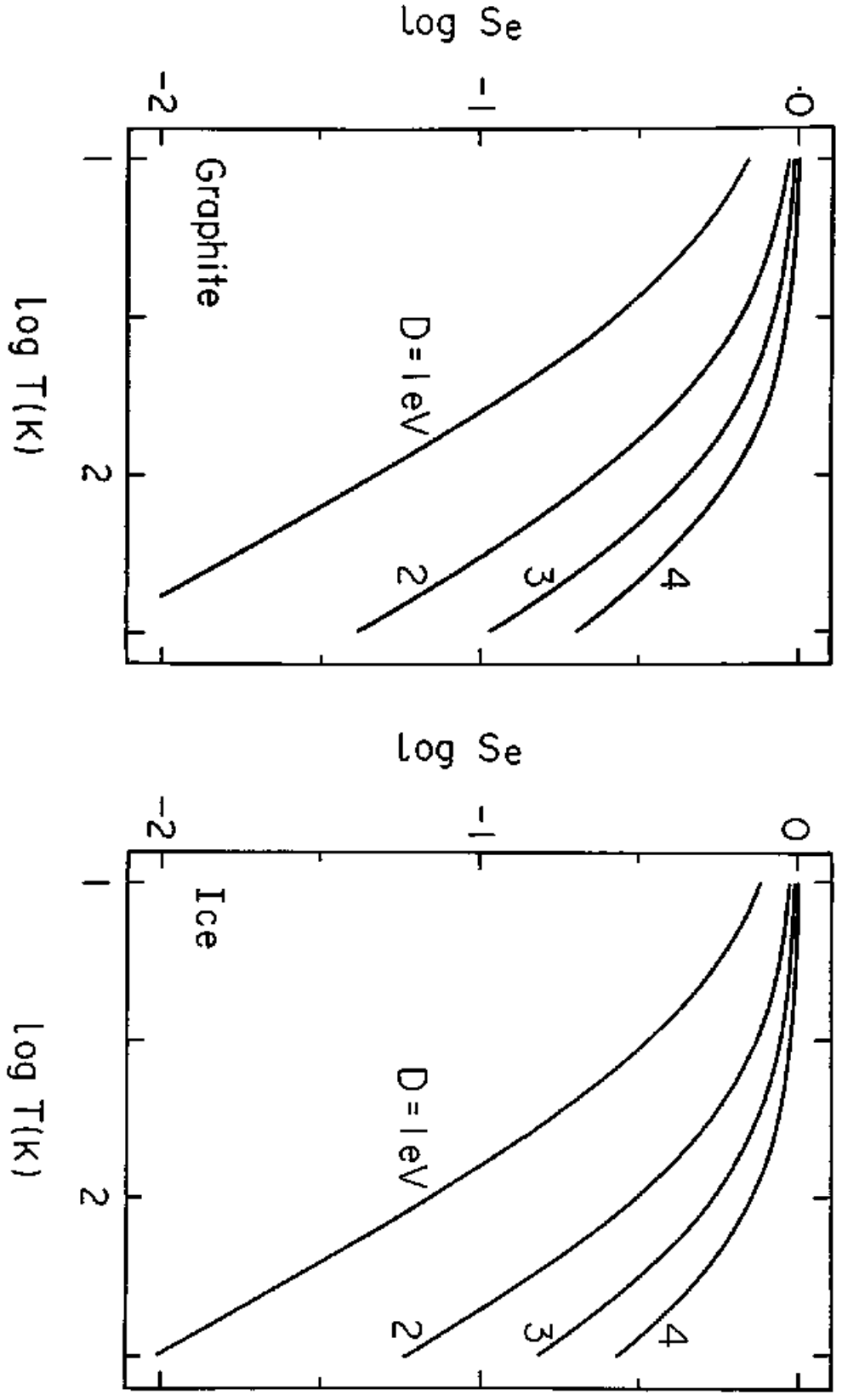
log Se
-2
-1
0
1
2
log T(K)
Graphite
D=1eV
2
3
4
log Se
-2
-1
0
1
2
log T(K)
Ice
D=1eV
2
3
4

Fig. 1

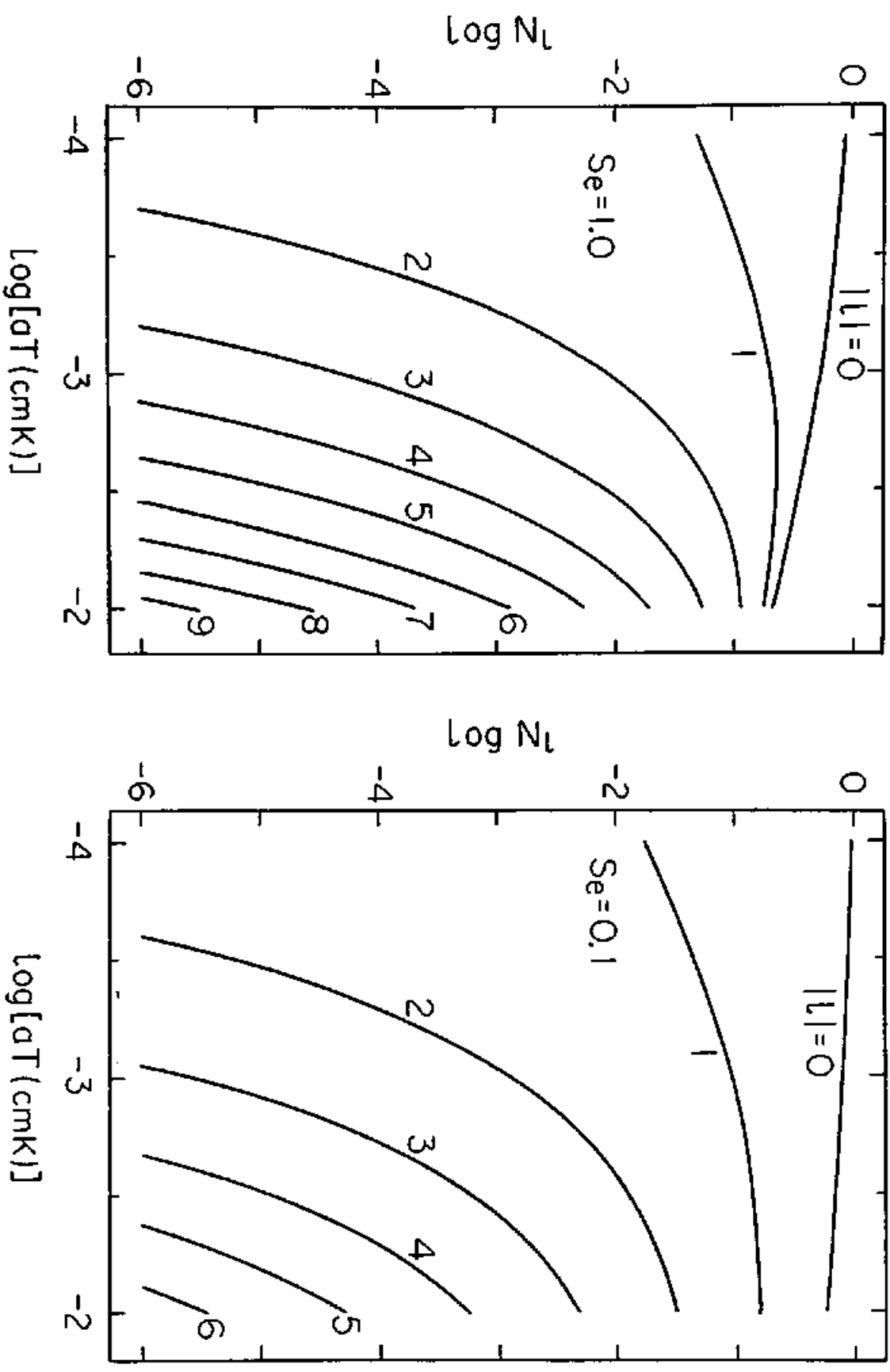
Log N_L
0
-2
-4
-6
Se=1.0
|1|=0
1
2
3
4
5
6
7
8
9
Log[aT(cmK)]
-2
-3
-4
Log N_L
0
-2
-4
-6
Se=0.1
|1|=0
1
2
3
4
5
6
Log[aT(cmK)]
-2
-3
-4

Fig. 2

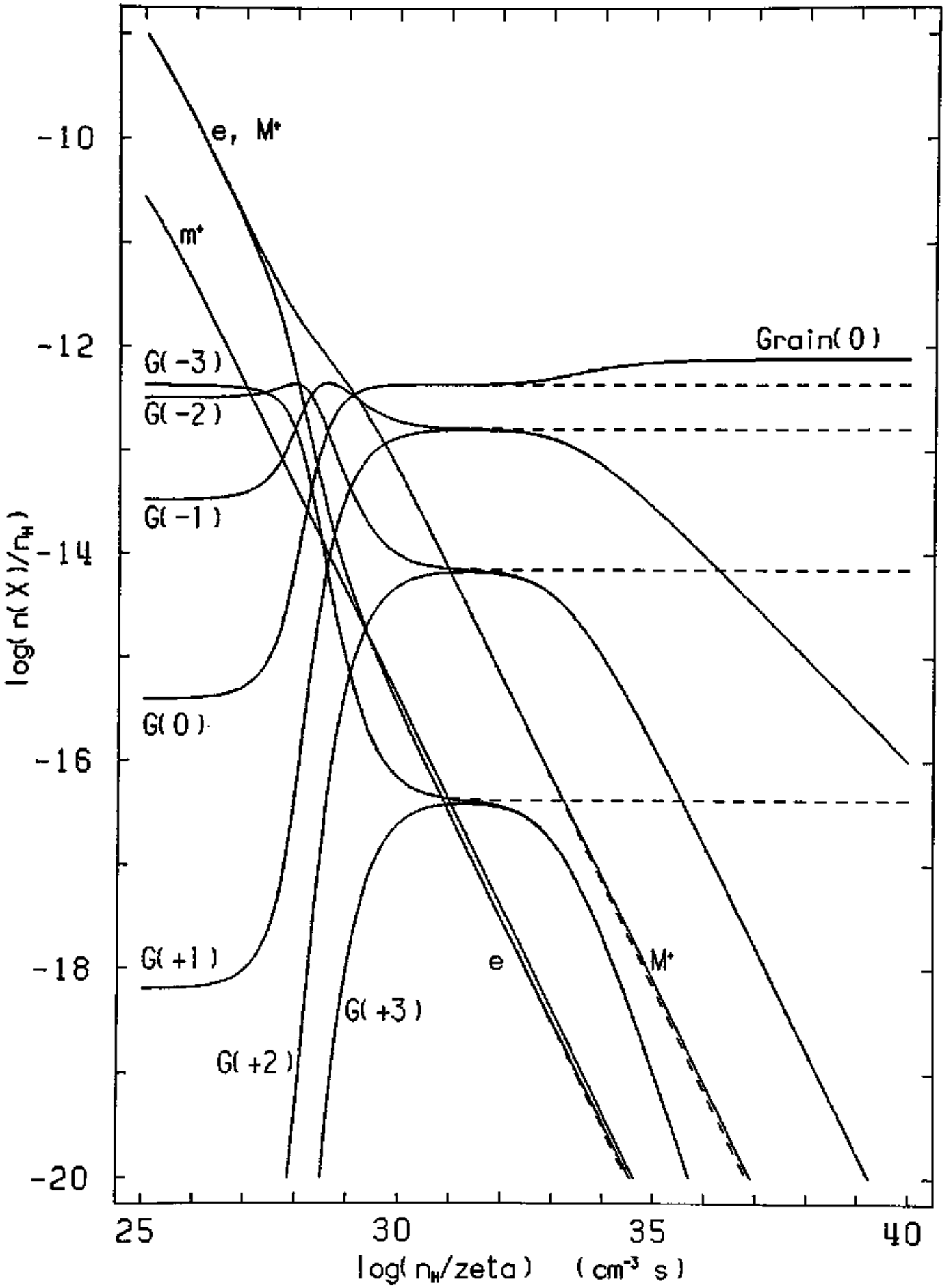
e, M+
m+
Grain(0)
G(-3)
G(-2)
G(-1)
G(0)
G(+1)
G(+2)
G(+3)
e
M+
-10
-12
-14
-16
-18
-20
25
30
35
40
log(n(X)/n_H)
log(n_H/zeta) (cm^-3 s)

Fig. 3

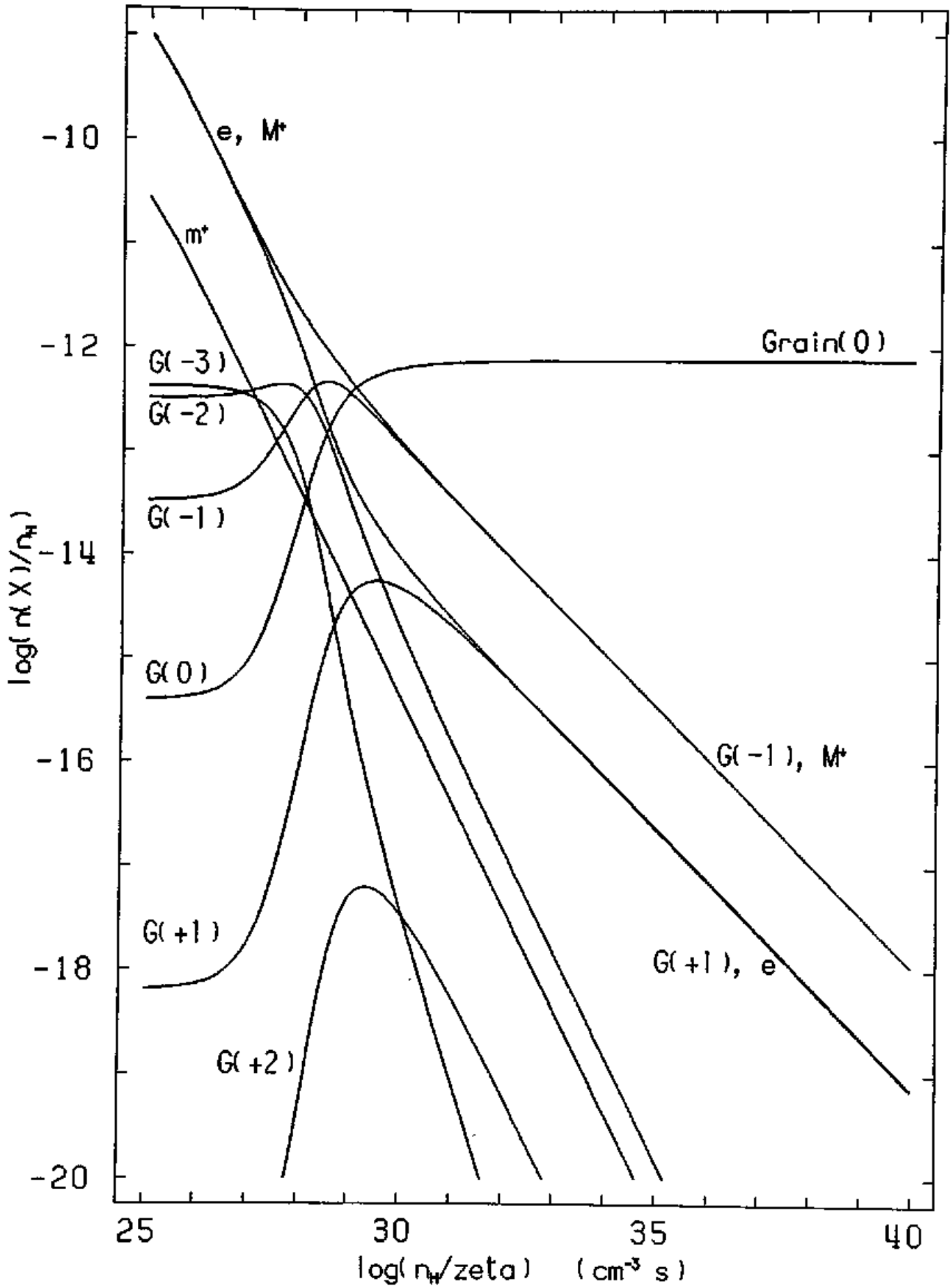
e, M+
m+
Grain(0)
G(-3)
G(-2)
G(-1)
G(0)
G(-1), M+
G(+1)
G(+1), e
G(+2)
-10
-12
-14
-16
-18
-20
log(n(X)/nH)
25
30
35
40
log(nH/zeta) (cm-3 s)

Fig. 4

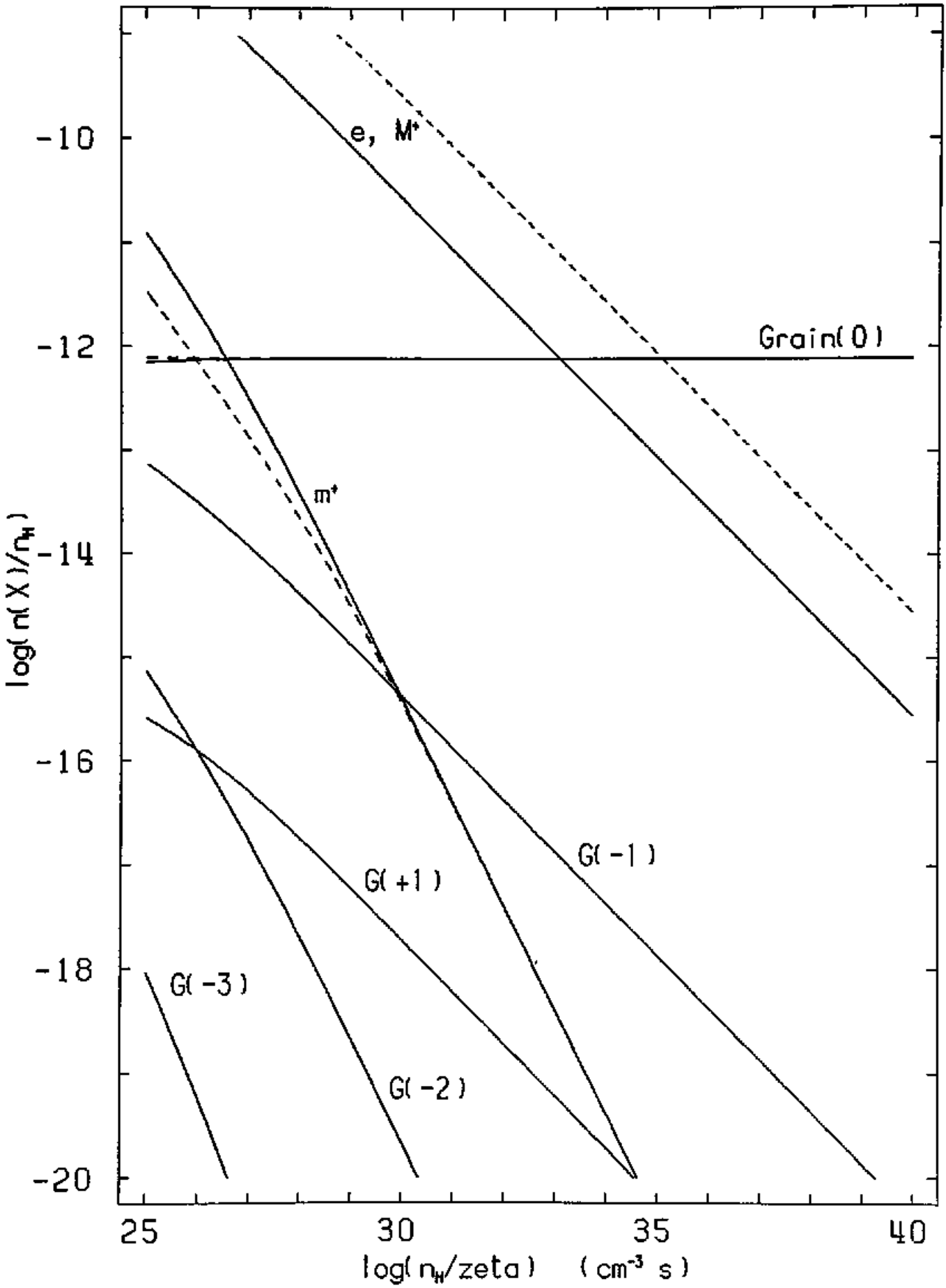
e, M+
Grain(0)
m+
G(-1)
G(+1)
G(-3)
G(-2)
-10
-12
-14
-16
-18
-20
25
30
35
40
log(n(X)/nH)
log(nH/zeta) (cm-3 s)

Fig. 5

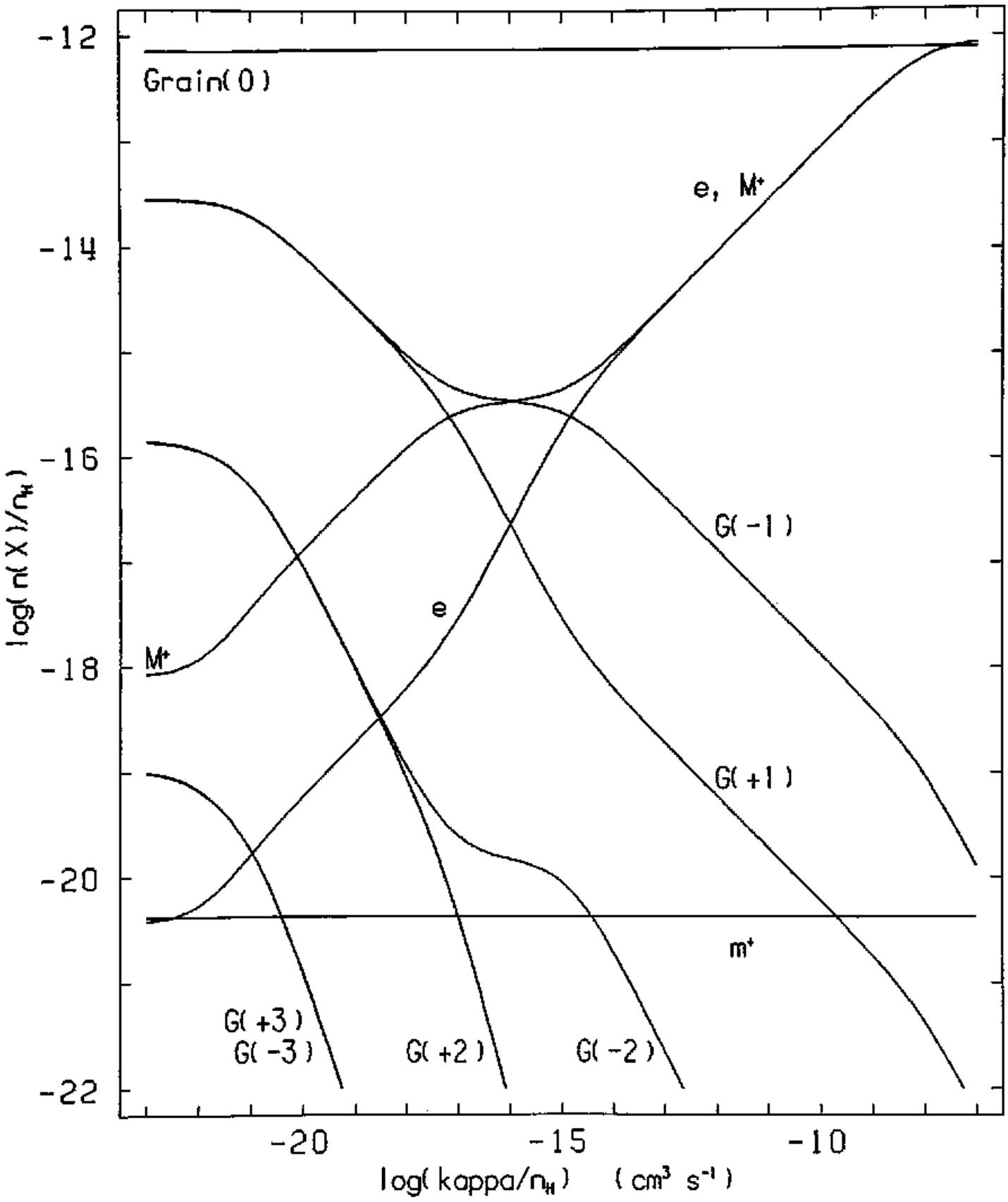
-12
-14
-16
-18
-20
-22
log(n(X)/n_H)
Grain(0)
e, M+
G(-1)
e
M+
G(+1)
m+
G(+3)
G(-3)
G(+2)
G(-2)
-20
-15
-10
log(kappa/n_H) (cm^3 s^-1)

Fig. 6

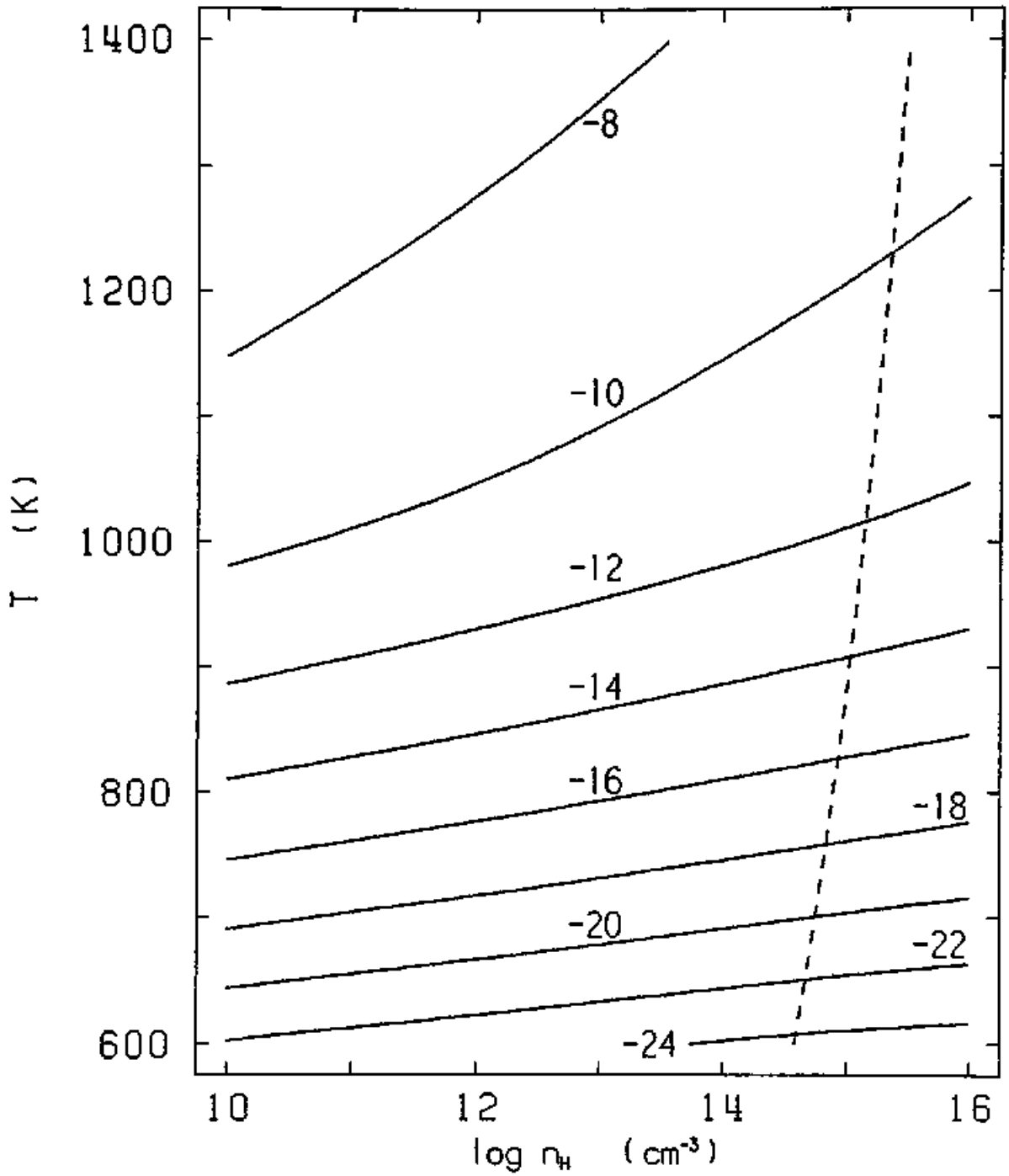
1400
1200
1000
800
600
T (K)
-8
-10
-12
-14
-16
-18
-20
-22
-24
10
12
14
16
log n_H (cm^{-3})

Fig. 7

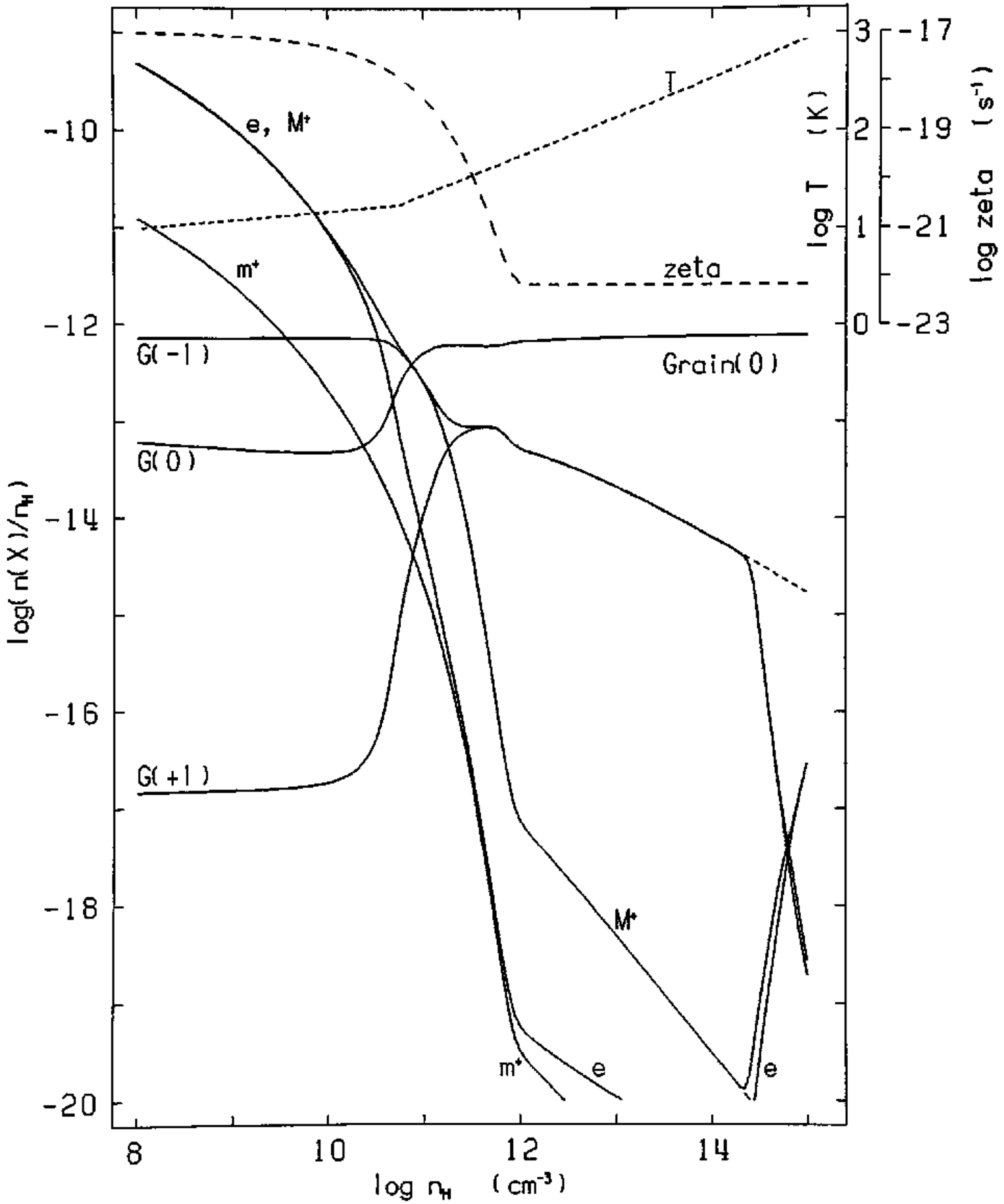
e, M+
m+
G(-1)
G(0)
G(+1)
I
zeta
Grain(0)
M+
m+
e
e
log T (K)
log zeta (s-1)
log(n(X)/nH)
log nH (cm-3)
-10
-12
-14
-16
-18
-20
8
10
12
14
3
2
1
0
-17
-19
-21
-23

Fig. 8

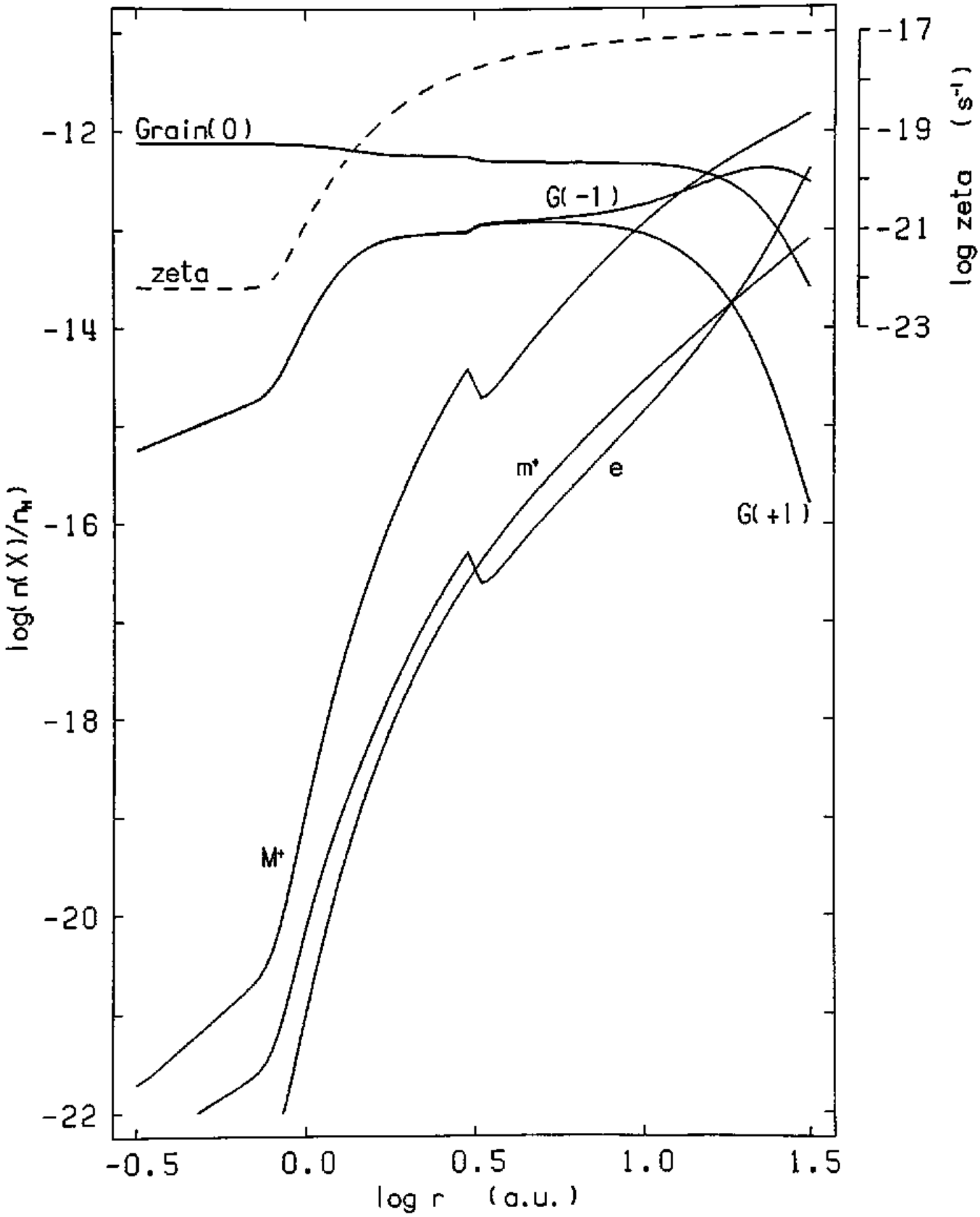
Grain(0)
G(-1)
zeta
m+
e
G(+1)
M+
-12
-14
-16
-18
-20
-22
-17
-19
-21
-23
log zeta (s⁻¹)
log(n(X)/nH)
-0.5
0.0
0.5
1.0
1.5
log r (a.u.)

Fig. 9